Insights into the contact point mobility of the railway superstructure treated as a periodic medium

D. Tallarico, B. Van Damme, L. Taenzer, A. Bergamini
EMPA, Laboratory for Acoustics/Noise control,
Überlandstrasse 129, 8600, Dübendorf, Switzerland
e-mail: **domenico.tallarico@empa.ch**

Abstract
Railway superstructures are, together with train wheelsets, the main source of structure-borne noise during a train pass-by. Understanding their detailed dynamic response is therefore of paramount importance to conceive noise abatement and structural health monitoring solutions. In this paper, we report on a method to numerically synthesize the dispersion information of the railway superstructure into its dynamic response to a point load - a train wheel, for example. With the help of commercial finite element routines, and exploiting Bloch-Floquet analysis, only a unit-cell is required in order to describe how an harmonic load evolves in space away from the loading region. The research is relevant for (a) singling-out the noise contribution coming from the rail superstructure; (b) estimating the wheel-rail dynamic contact forces; (c) providing a flexible algorithm able to tackle novel by-design components for effective railway noise and vibration control.

1 Introduction

The railway superstructure comprises a - practically infinite - periodic repetition of sleepers supporting the rail. In this sense, the theory of Bloch-Floquet waves - which is at the basis of the description of periodic media - meets in a direct way an engineering structure. Despite that, models of railway dynamics either rely on homogenised supports (i.e. no periodicity) or transfer matrix models accounting for periodicity via an infinite set of equations that has to be truncated. The elegance and power of Bloch-Floquet theory combined with Green's function approaches - that predict the dynamic response to an impulsive load - has only been applied to railway systems in few semi-analytical cases. In this context, we mention the work by Heckle [1], whose focus was on the construction of the quasi-periodic Green's function for a single Timoshenko beam (representing a rail), supported by discrete elastic elements (representing the pad-sleeper system). A different but relevant model problem (i.e. a periodically supported bridge), was considered by Brun *et al.* [2] where the focus was on the Wiener-Hopf formulation (and related Green's kernels) of a moving fault. Differential operators very seldom admit a simple, closed form expression for the Green's function. This explains why Green's function-based techniques are so rare in practical contexts, such as in the modelling of elongated periodic engineering infrastructures. In the context of high-frequency noise emission, Wu and Thompson [3] proposed a homogeneously supported double Timoshenko beam model, whose Green's function was calculated using integral transform techniques. To improve accuracy, the cross-section of a three-dimensional (3D) rail was accounted for in [4] within an elegant 2.5D model for the rail interacting with a finite set of sleepers via a transfer matrix approach.

To the best of our knowledge, the construction of the finite element quasi-periodic Green's function of a 3D rail superstructure is still missing. The following question inspires the present conference paper: how to combine the elegance of Bloch-Floquet theory and the resulting dispersion information of periodic structures with the response of such periodic structures to external loads?

The aim of this contribution is to show-case a reconciliation between finite element (FE) unit-cell modelling, Bloch-Floquet theory and Green's function techniques, in the context of the railway infrastructure. A discus-

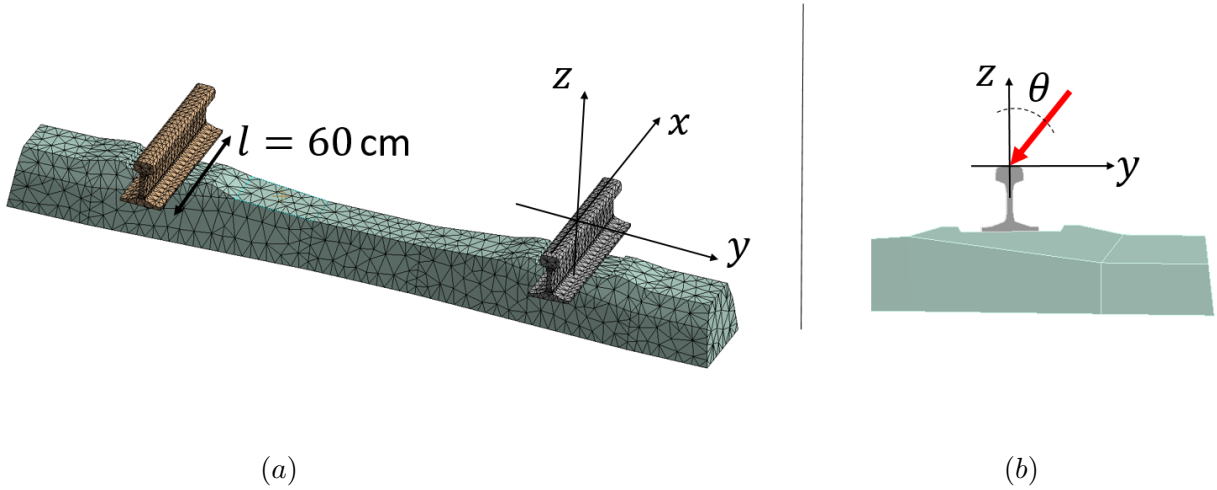

(a) (b)

Figure 1: Panel (a) represents the unit-cell of the railway superstructure, whereas panel (b) shows the force in red.

sion on the compatibility equations leading to the results is beyond the scope of the present manuscript. The reader is referred to previous inspiring work by Duhamel [5] and to forthcoming articles by the corresponding author. Here, we focus on illustrating the general work-flow that, from dispersion information (Fig. 2), leads to the point-wise (Figs. 3 and 5) and full-field (Fig. 4) dynamic response of the railway superstructure.

2 Modelling assumptions and outline of the algorithm

The method relies on the finite element (FE) discretization of a *single* unit cell of the railway superstructure (see Fig. 1(a)). We separately model the sleeper and rail as linear elastic solids in the time-harmonic regime. The material parameters are listed in Tab. 1. Compatibility between the rail and sleepers is guaranteed by a set of springs which represents rail-pads. In addition, the sleeper bottom surface rests on a set of grounded springs which act as an elastic foundation, similarly to the ballast bed (see elastic parameters in Tab. 1).

The effect of the periodicity is captured by prescribing Bloch-Floquet boundary conditions on the assembled linear algebraic equations of the unit cell. In the framework of the direct Bloch-Floquet method [6, 7], the 1D translational symmetry results in a second-degree polynomial eigenvalue problem in the Bloch parameter k, whose solution is a set of complex wave-numbers $\mathcal{K}(\omega)$ and associated eigenvectors ψ_k with $k \in \mathcal{K}(\omega)$ and ω the radian frequency. Here, ψ_k is a nodal vector with the same dimensionality as the master Bloch-Floquet

Table 1: Elastic parameters for modelling the various rail components. The damping ratio is intended as a scalar controlling the structural damping of the sleeper. E, ν and ρ are Young's modulus, Poisson's ratio and mass density, respectively.

	E [GPa]	ν [-]	ρ [kg/m^3]	Lat. Stiffness [MN/m]	Vert. Stiffness [MN/m]	Damp. Ratio [-]
Sleeper	46.3	0.2	2435.6	-	-	0.05
Rail	200	0.3	7850	-	-	-
Rail-pads	-	-	-	$30(1+0.15i)$	$610(1+0.25i)$	-
Ballast	-	-	-	-	$27.5(1+2i)$	-

degrees of freedom (dofs) which - consistently with the choice of the unit cell in Fig. 1(a) - are located on the rail. From a computational point of view, since the dimensionality of the master dofs is relatively small compared to the dofs size of the unit cell, the most time consuming step is the dynamic condensation needed

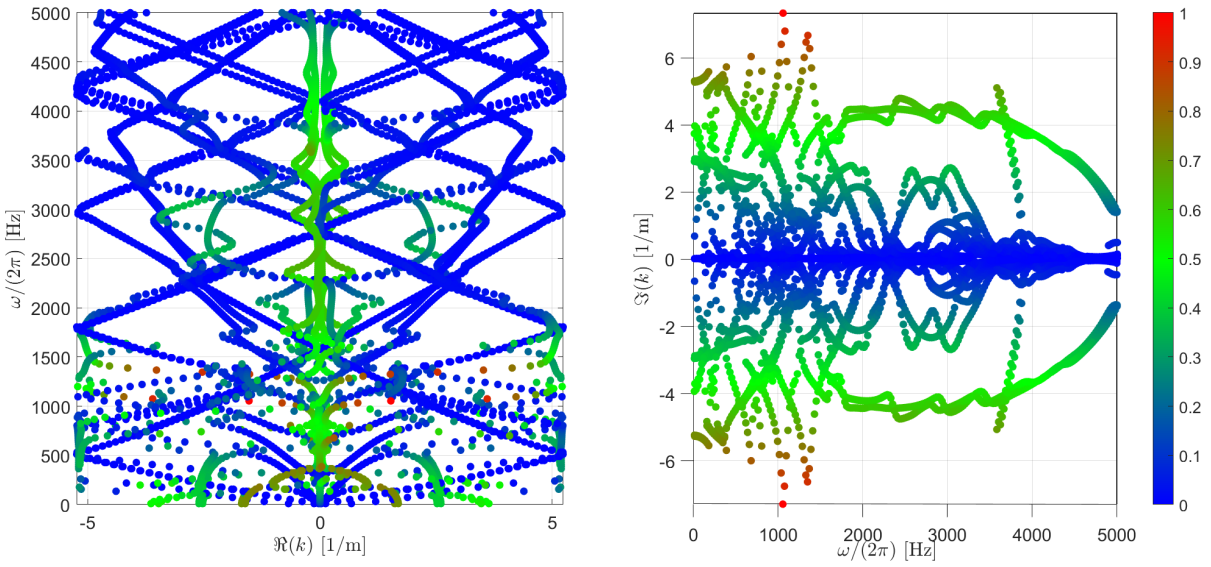

Figure 2: Projection of the complex dispersion diagrams into the ω-$\Re(k)$ (panel (a)) and ω-$\Im(k)$ (panel (b)) planes. The colour scale represents $\xi = |\Im(k)/k_0|$ with k_0 chosen to be $k_0 = 7.5$ 1/m.

to project the equations of the unit cell onto Bloch-Floquet master nodes. In order to alleviate this cost, an effective model-order reduction technique has recently been proposed [8].

For each ω, the solution of the displacement in the periodic medium can be represented as

$$\psi(\omega) = \sum_{k \in \mathcal{K}(\omega)} a_k \psi_k, \tag{1}$$

i.e. a summation over the Bloch-Floquet eigenmodes. The compatibility with an external time-harmonic force

$$\mathbf{F}_0(x, y, z) = F_0 \begin{pmatrix} 0 \\ \sin(\vartheta) \\ -\cos(\vartheta) \end{pmatrix}, \tag{2}$$

concentrated in a node on the top of the rail (see Fig. 1(b)), allows to calculate the coefficients a_k in Eq. (1). The minimal representation in Eq. (1) can be expanded into internal nodes of the unit-cell (including the node where the force is applied), knowing the matrix equations for dynamic condensation, and in adjacent cells via Bloch-Floquet shifts.

3 Results

3.1 Dispersive properties

Fig. 2 shows the complex dispersive properties of the unit cell in Fig. 1 with material parameters as in Tab. 1. The data are organized according to the caption. Panel (a) is bound to the first Brillouin zone (FBZ) of the railway, *i.e.* $\Re(k) \in [-5.23, 5.23]$ 1/m.

For reference, the blue dots in panel (a) are the classic dispersion diagrams that can be obtained from the indirect Bloch-Floquet method in the absence of damping. The most striking feature is perhaps the folding behaviour of the (super-linear) flexural modes happening at the boundaries of the boundaries of the FBZ, in conjunction with a plethora of modes hybridised with the sleeper local resonances below 1500 Hz. This latter

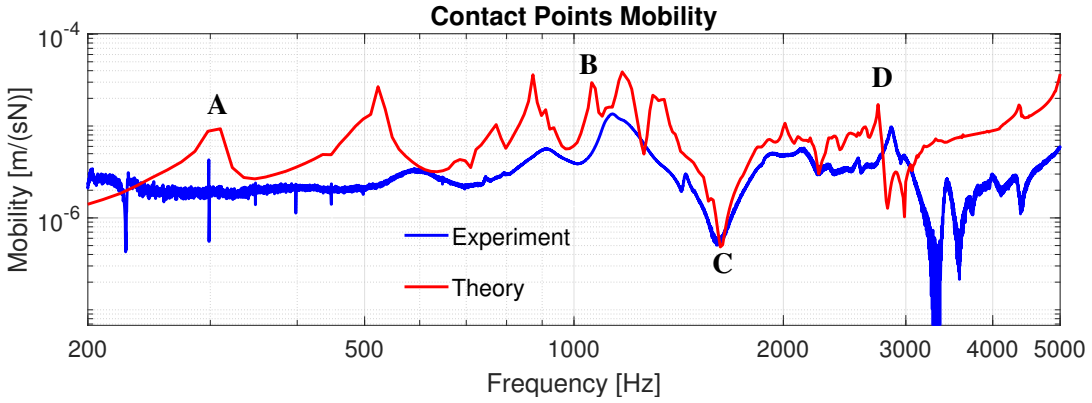

Figure 3: Comparison of experimental and numerical railway contact point mobility. The letters identify special resonances and anti-resonances whose full field representation is given in Fig. 4.

effect is further visible in panel (b) whereby the imaginary part features highly resonant behaviour typical of locally resonant metamaterials [9]. Local resonances are provided here by the sleepers' eigenmodes.

3.2 Contact point mobility

As outlined in Sec. 2, the dispersion information is distilled into the dynamic response of the railway superstructure to an external load as in Eq. (2). We begin by comparing the experimental results obtained on a real railway, during a measurement campaign in Effretikon (CH). The track has a typical structure used by SBB, having B91 concrete sleepers, stiff rail pads made out of EVA, W14 rail clamps by Vossloh, and steel 60E2 rails. The focus is on the contact point mobility of the railway which has been experimentally obtained via measurements carried out via a shaker instrumented with an impedance head, placed at $(x, y, z) \approx (-20, 0, 0)$ cm (see reference system in Fig. 1) and acting vertically ($i.e.$ $\vartheta = 0$ in Eq. (2)). The impedance head can measure force $F(t)$ and acceleration $a(t)$ time series, that have been Fourier transformed ($\tilde{F}(\omega)$ and $\tilde{a}(\omega)$, respectively) and converted into a mobility transfer function as

$$\mu_{\text{exp}}(\omega) = \frac{1}{\omega} \left| \frac{\tilde{a}(\omega)}{\tilde{F}(\omega)} \right| . \tag{3}$$

A similar information can be obtained from the model as

$$\mu_{\text{theo}}(\omega) = \omega \left| \frac{\psi_0(\omega)}{F_0} \right| , \tag{4}$$

where ψ_0 represents the displacement nodal degree of freedom at the excitation node, in the vertical direction.

Fig. 3 shows the comparison of the prediction (red line) with the measured transfer function (blue line), assuming a configuration similar to that of the experiment. We can observe that the behaviour of the mobility is very well captured by the FE Green's function model, at all frequencies up to 5000 Hz. In particular, below 1000 Hz several pronounced resonances appear associated with sleeper modes, in fair agreement with what is observed experimentally. Around 1100 Hz, the experimental mobility reaches a maximum associated with a pinned-pinned resonance where the sleepers are believed to effectively act as pinning support for the rail. A plethora of resonances and anti-resonances follow, all captured by the prediction.

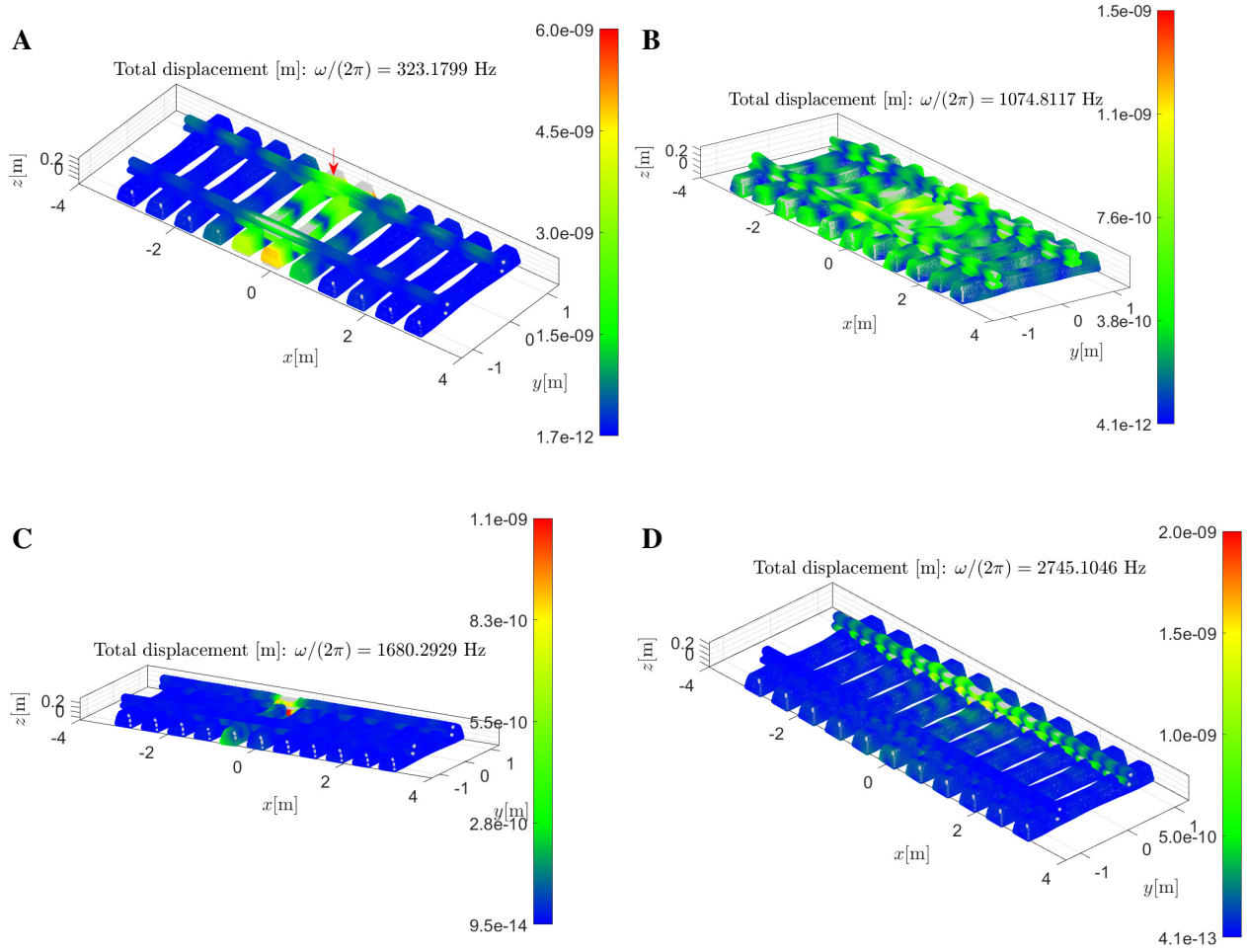

Figure 4: . Selected waveforms comprising five sleepers around the fundamental unit cell where the harmonic load is applied (see vertical red arrow in panel **A**). Different panels correspond to different frequencies, marked for convenience in Fig. 3.

3.3 Waveforms

To shed light on the nature of such resonances, we report in Fig. 4 a set of selected waveforms. Fig. 4**A** clearly shows that the waveform is dominated by an antisymmetric sleeper mode. Waves quickly decay away from the excitation point, due to the sleeper damping. In Fig. 4**B**, the waveform shows the typical "pinned-pinned" resonance, some sleepers away from the excitation point. We observe that, although the harmonic load is concentrated in one rail, the elasticity of the sleeper transmits vibrations to the adjacent rail. This phenomenon is disregarded in single-rail models and may be of relevance for future experimental campaigns. Higher frequency waveforms are represented in Fig. 4**C** and 4**D**, displaying highly localised and propagating behaviour, respectively. Although this may look unusual, this is entirely consistent with the solution Ansatz in Eq. (1), as the summation includes purely propagating as well as left and right decaying waves. This is in turn consistent with the dispersion diagrams in Fig. 2.

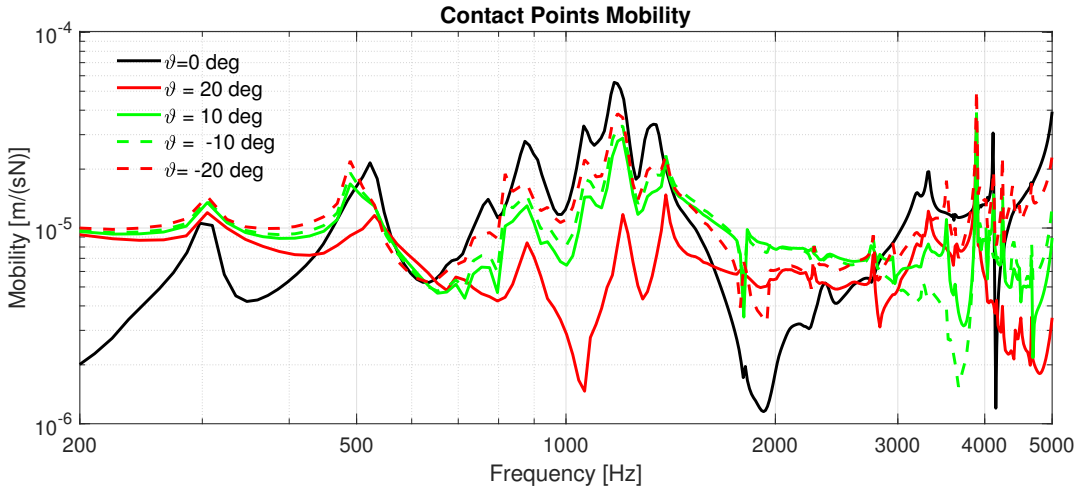

Figure 5: Comparison of the numerical vertical contact point mobility as the angle of attack in Eq. (2) is varied.

3.4 Effect of the angle of attack

Fig. 5 shows the vertical contact point mobility as a function of frequency, for different angles of attack of the force vector. The situation is illustrated in Fig. 1(b) and modelled as in Eq. (2). The force is applied at $(x, y, z) \approx (-29, 0, 0)$ cm with respect to the reference system in Fig. 1(a). This point is the nearest internal node to the so-called midspan of the railway which coincides with the Bloch-Floquet master nodes. The analysis reported in Fig. 5 emulates situations encountered in curves, where the wheelsets exert forces under an angle with respect to the vertical, positive (negative) for right (left) turns in the direction of travel. The diagram shows that the angle of the force has an enormous effect on the prediction of the vertical contact point mobility. This may be of relevance in future work focusing on noise emissions from bends in the railway.

4 Conclusion and outlook

In conclusion, we have shown that the dispersive properties of the railway superstructure can be distilled into its finite-element Green's function, allowing the prediction of the contact point mobility, an essential ingredient for estimating of the wheel/rail dynamic contact forces. The predicting power of the method is of course limited by the accurate prescription of the linear-elastic material properties of the subcomponents. To this end, the accurate modelling of the subcomponent informed by experimental insights is essential. For example, higher damping within the sleepers or frequency-dependent ballast and rail-pad elastic properties, may improve the agreement with experiments. The determination of best-fitting parameters is however beyond the scope of the manuscript, as the focus has been here on the ineherent frequency dependency of the contact-point mobility due to periodicity-induced dispersive behaviour of the railway, triggered by localised forces, under several angle of attack. The method will be exploited for the prediction of more sophisticated railway noise indicators, such as the track decay rate and sound levels. In a broader perspective, coupling the present method with optimization schemes may unveil novel by-design properties of periodic structures and their truncations, possibly incorporating radiation into acoustic fields.

Acknowledgements

The work has been commissioned and funded by the Ministry of Environment of the Swiss Confederation (FOEN) under project sonRAIL2x (contract number 1337000438).

References

[1] M. A. Heckl, "Coupled waves on a periodically supported timoshenko beam," *Journal of Sound and Vibration*, vol. 252, no. 5, pp. 849–882, 2002.

[2] M. Brun, A. B. Movchan, and L. I. Slepyan, "Transition wave in a supported heavy beam," *Journal of the Mechanics and Physics of Solids*, vol. 61, no. 10, pp. 2067–2085, 2013.

[3] T. Wu and D. Thompson, "A double timoshenko beam model for vertical vibration analysis of railway track at high frequencies," *Journal of Sound and Vibration*, vol. 224, no. 2, pp. 329–348, 1999.

[4] X. Zhang, D. J. Thompson, Q. Li, D. Kostovasilis, M. G. Toward, G. Squicciarini, and J. Ryue, "A model of a discretely supported railway track based on a 2.5 d finite element approach," *Journal of Sound and Vibration*, vol. 438, pp. 153–174, 2019.

[5] D. Duhamel, "Finite element computation of green's functions," *Engineering Analysis with Boundary Elements*, vol. 31, no. 11, pp. 919–930, 2007.

[6] M. Collet, M. Ouisse, M. Ruzzene, and M. Ichchou, "Floquet–bloch decomposition for the computation of dispersion of two-dimensional periodic, damped mechanical systems," *International Journal of Solids and Structures*, vol. 48, no. 20, pp. 2837–2848, 2011.

[7] B. R. Mace and E. Manconi, "Modelling wave propagation in two-dimensional structures using finite element analysis," *Journal of Sound and Vibration*, vol. 318, no. 4-5, pp. 884–902, 2008.

[8] D. Tallarico, G. Hannema, M. Miniaci, A. Bergamini, A. Zemp, and B. Van Damme, "Superelement modelling of elastic metamaterials: Complex dispersive properties of three-dimensional structured beams and plates," *Journal of Sound and Vibration*, vol. 484, p. 115499, 2020.

[9] M. I. Hussein, M. J. Leamy, and M. Ruzzene, "Dynamics of phononic materials and structures: Historical origins, recent progress, and future outlook," *Applied Mechanics Reviews*, vol. 66, no. 4, 2014.